Thermal response of a nanoscale hot-wire in subsonic and supersonic flows

Florian Brunier-Coulin, Diogo C Barros, Alexander Piqué, Marcus Hultmark, Pierre Dupont

▶ **To cite this version:**

Florian Brunier-Coulin, Diogo C Barros, Alexander Piqué, Marcus Hultmark, Pierre Dupont. Thermal response of a nanoscale hot-wire in subsonic and supersonic flows. Experiments in Fluids, 2022, 10.1007/s00348-022-03545-z . hal-04311504

HAL Id: hal-04311504
https://amu.hal.science/hal-04311504

Submitted on 30 Nov 2023

HAL is a multi-disciplinary open access archive for the deposit and dissemination of scientific research documents, whether they are published or not. The documents may come from teaching and research institutions in France or abroad, or from public or private research centers.

L'archive ouverte pluridisciplinaire **HAL**, est destinée au dépôt et à la diffusion de documents scientifiques de niveau recherche, publiés ou non, émanant des établissements d'enseignement et de recherche français ou étrangers, des laboratoires publics ou privés.

Experiments in Fluids manuscript No.
(will be inserted by the editor)

Thermal response of a nanoscale hot-wire in subsonic and supersonic flows

Florian Brunier-Coulin · Diogo C. Barros · Alexander Piqué
Marcus Hultmark · Pierre Dupont

Received: date / Accepted: date

Abstract A comprehensive characterization of the thermal response of nanoscale hot-wire probes is performed in both subsonic and supersonic flows. A constant current anemometer was designed for the measurement of the intrinsic thermal inertia of hot-wire probes. In particular, the nanoscale probe is considered with the effect of gold-plating on supporting structure of the targeted sensing element. Gold-plated nanoscale probes present a response time one order of magnitude smaller than conventional cylindrical hot-wire probes. Heat transfer simulations show that the temperature profile is considerably modified by the addition of a conductive metal layer, hence increasing the sensor's frequency response in both subsonic and supersonic flows. The increase of frequency response is finally exemplified by the numerical computation of the power spectral density of a turbulent flow signal without any electric compensation of the hot-wire signal.

Keywords Hot-wire anemometry · Frequency response · Thermal response

1 Introduction

Hot-wire anemometry has become an ubiquitous tool for the investigation of turbulent flows since the pioneering work of King (1914). The small dimension of the probes is associated with high spatial and temporal resolution, making them appropriate for the characterization of unsteady flows both in subsonic and supersonic applications (Kovasznay, 1950; Comte-Bellot, 1976).

Conventional hot-wire probes consist of cylindrical tungsten or platinum wires with active length and diameter on the order of 1 mm and 5 μm, respectively. Novel fabrication methods in microelectromechanical systems (MEMS) have paved the way for the design of nanoscale thermal anemometry probes (NSTAP) targeting highly resolved measurements in a variety of flow conditions (Bailey et al, 2010; Vallikivi and Smits, 2014; Kokmanian et al, 2019; Le-The et al, 2021). The deposition of controlled thin metal layers makes possible the design of smaller probes with a well defined geometry to increase both time and spatial resolution of turbulent flow measurements (Bailey et al, 2010).

While the frequency response of the NSTAP probes operated in constant temperature anemometry (CTA) has been investigated in previous experiments (Hutchins et al, 2015; Kokmanian et al, 2021), the intrinsic thermal inertia, and corresponding open loop response of such hot-wire probes have not been characterized systematically. In CTA anemometers, the probe resistance, hence its temperature, is kept constant by a feedback loop in the circuit that imply current variations to compensate for the flow unsteadiness and the probe's thermal inertia. In constant current (CCA) systems, a targeted electric current traverses the wire, whose electric resistance varies due to flow unsteadiness. A step change of flow velocity or temperature, for example, would imply a voltage response across the wire. The time lag of this response is associated with the intrinsic wire thermal inertia when no electrical compensation is applied within the circuit.

The possibility to combine materials with different thermal and electrical properties to modify the local response of the NSTAP probes has never been explored. In this work, this approach is implemented to optimize the intrinsic ther-

Florian Brunier-Coulin, Diogo C. Barros and Pierre Dupont
Aix Marseille Université, CNRS, IUSTI, Marseille, France
E-mail: diogo.camello-barros@univ-amu.fr

Florian Brunier-Coulin
Le Havre Université, CNRS, LOMC, Le Havre, France

Alexander Piqué and Marcus Hultmark
Department of Mechanical and Aerospace Engineering
Princeton University, Princeton, USA

mal response of nanoscale probes in both subsonic and supersonic flow conditions. The probes studied here are an extension of the nanoscale probes examined in Kokmanian et al (2021), which have been proved robust to supersonic flow conditions. The time constant of the probes was measured by the use of square-wave tests in a CCA system specifically designed for this study. In section 2, we present the electronic characteristics of the CCA system, the details about the NSTAP probes and the employed aerodynamic flow configurations. Section 3 describes the square-wave tests and the time constant results. A heat transfer analysis is performed in section 4 to explain the probe temperature profile and main results. Finally, section 5 provides an example of a turbulent flow measurement and associated numerical compensation using a theoretical model employing the measured time response, followed by the concluding remarks in section 6.

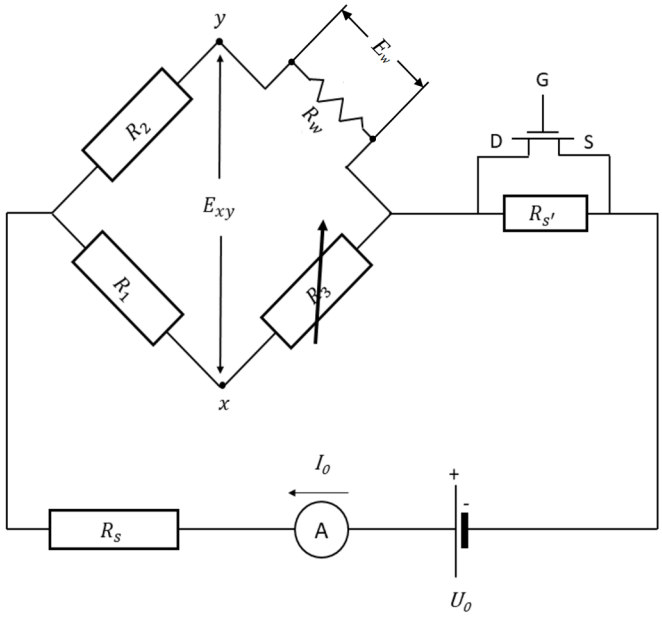

Fig. 1 Sketch of the constant current anemometer system.

2 Experimental setup

2.1 Anemometer system

A constant current anemometer (CCA) system was designed to measure the thermal response of the nanoscale probes. Figure 1 presents a sketch of all electrical components of the device. The hot-wire sensor, represented here by the resistance R_w, is connected within a Wheatstone bridge composed of two top resistances $R_1 = R_2 = 100\ \Omega$ and a third variable resistance R_3 in the range 0-100 Ω. This resistance was employed to set a target value of R_w when the bridge is perfectly balanced. The bridge is supplied by a constant current generator connected to the main resistance $R_s = 12\ \Omega$.

In order to generate periodic variations of the electrical current traversing the bridge, another resistance $R_{s'} = 3.5\ \Omega$ was installed with a MOSFET (metal oxide semiconductor field effect transistor) transistor. Supplying the transistor with a square-wave signal, thus short-circuiting the resistance $R_{s'}$, allows one to modify periodically the current I_o traversing the bridge. This method has been widely recognized to simulate a step change in flow velocity to determine the frequency response of hot-wire probes (Kovasznay, 1950; Bruun, 1995). Indeed, the thermal response of the sensing element is driven by the time needed for saturation following a step change of velocity. This duration corresponds to the time required to reach the equilibrium between the heat transfer from the Joule effect in the sensing element and the heat exchange with the flow. This approach differs from the frequency response test in a CTA system, in which the wire signal is intrinsically compensated to maintain a constant probe temperature (Hutchins et al, 2015)).

For each measurement, by varying R_3 and balancing the bridge, we set the value of R_w to obtain a known overheat resistance ratio $a_w = (R_w - R_e)/R_e$. Here, R_e is the equilibrium resistance of the unheated wire in the flow. The procedure consists in adjusting the supply current while the equilibrium of the Wheatstone bridge is maintained by adjusting R_3. The bridge voltage E_{xy} is proportional to the variation of the probe resistance R_w. In this configuration, the variation of the voltage corresponding to the response of the sensing element is measured along the power input of the hot wire. It implies a lower signal-to-noise ratio (SNR) when compared to the direct measurement of E_w variations, but the equilibrium condition of the Wheatstone bridge allows a direct amplification of E_{xy} with a differential amplifier, limiting the number of electronic components. In addition, as described in section 3.1, a phase average is conducted to highlight only the periodic variation of R_w. During the square wave tests, E_{xy} was monitored to record the time response of the sensor due to the step changes in the bridge traversing current.

It is important to note that the present anemometer does not apply any electrical compensation to the bridge voltage. Hence, the measured signal response corresponds to the intrinsic thermal lag of the probes.

2.2 Hot-wire probes

The nanoscale thermal anemometry probes (NSTAP) investigated in the current experiments are an extension of the sensors explored in Kokmanian et al (2021). In figure 2, we present a microscope image of the sensor's tip. It consists of a platinum nanoscale ribbon sensing element with length $30\,\mu$m and $2\,\mu$m wide. This sensing element is supported by two triangular platinum structures, which are held by longer

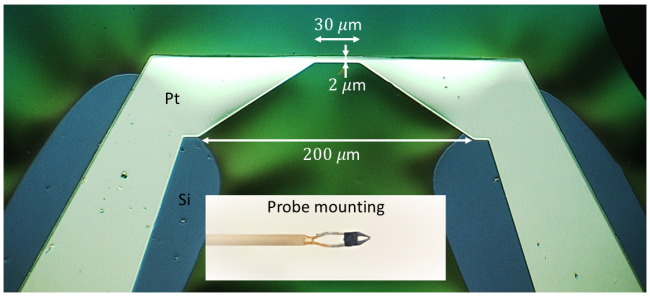

Fig. 2 Microscope photography of the NSTAP probe's tip consisting of a 300 nm-platinum layer (Pt) deposited on a silicon (Si) wafer.

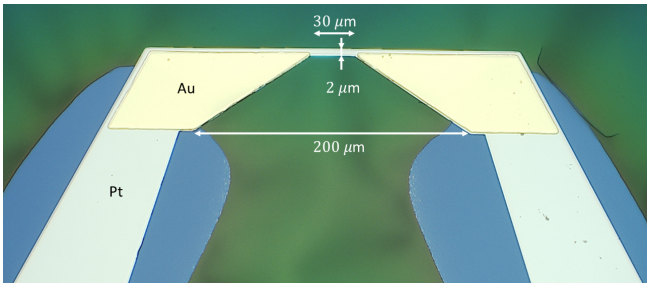

Fig. 3 Gold-plated NSTAP probe. The gold layer thicknesses considered are 200 nm and 360 nm.

platinum prongs with a total length of 4 mm supported by a silicon base. The thickness of the entire platinum structure is 300 nm. Further details about the fabrication steps and the full geometry of the sensor can be found in Kokmanian et al (2019). The design of the sensors takes into account its operation in high-speed flows. Indeed, the continuous variation of the width of the triangular supports and the location of the sensing element at the most upstream position limit the effects of the existing shock waves in supersonic flow conditions.

Given that the entire platinum structure represents a unique electrical resistance, it is natural to inquire to what extent the triangular supports impact the thermal lag of the entire sensor. To quantify the role of this structure on the sensor's thermal response, layers of gold (Au) were superposed specifically over the triangular supports of the sensing element. The gold layer starts at the end of the sensing element and covers the supports until they reach a width of approximately 50 μm, where the heat generation is negligible due to the large cross section (see figure 3). In addition, the end of the gold layer coincides approximately with the silicon substrate that plays the role of a heat sink. In the following, two gold-plated configurations with gold thickness 200 nm and 360 nm will be considered together with the original platinum sensor. The gold was added on top of the 300 nm thick platinum structure.

The thermal response of a hot-wire probe depends directly on the electrical resistance of the sensor's body. Due to the more complex geometry of the NSTAP when compared to a conventional cylindrical hot-wire probe, it is difficult to estimate precisely the resistance of the entire platinum structure. Also, measuring the electrical resistance of the sensing element is very challenging due to its small dimension. An estimation of the sensor's resistance (see Kokmanian et al (2021) for the details of the entire geometry) based on the resistance of each section $R_i = \chi_0 l_i / S_i$ gives $R_w = 16\ \Omega$, while the measured probe resistance at 20°C was $R_w = 24.3\ \Omega$. Here, χ_0 is the electrical resistivity at 20°C, S_i is the local cross-section and l_i the corresponding length of the element. In the presence of 200 and 360 nm gold thicknesses, the estimated theoretical resistances are 13.7 and 12.9 Ω, while the measured resistances are $R_w = 22.3\ \Omega$ and $R_w = 21.2\ \Omega$, respectively.

The addition of gold reduces the electrical resistance given the lower value of the gold electrical resistivity when compared to the platinum (see table 3). The difference between the estimated and measured values of R_w is presumably due to the choice of the platinum resistivity $\chi_0 = 1.1 \times 10^{-7}\ \Omega$m. This value corresponds to the bulk resistivity of the platinum for relatively thick metal sheets. It is known that the electrical resistivity of platinum increases exponentially as the nanoscale thickness decreases. Féry (1928) measured the origin of the resistivity growth for a thickness $t = 348$ nm, indicating that χ_0 should have a larger value for the current studied thickness $t = 300$ nm. This could explain the differences between the estimated and the measured values of R_w. In the following, the values of both R_e and R_w used for the calculation of a_w correspond to the resistance of the entire metallic structure (not only the sensing element).

Finally, a conventional cylindrical hot-wire probe was employed to provide a comparative basis of the thermal response. This probe is a tungsten wire of diameter 5 μm and length 800 μm soldered on classical Dantec prongs.

2.3 Flow configurations

Measurements of the NSTAP's thermal response time were performed in both subsonic and supersonic flow conditions. The subsonic configuration is a low-speed axisymmetric jet with exit nozzle diameter $D_1 = 30$ mm and jet maximum velocity equal to 5 m/s. Details about the flow field of this jet facility can be found in the experiments of Schreyer et al (2015). The probes were placed in the potential core of the jet at the centerline exit location.

Experiments in supersonic flow were performed in the continuous wind-tunnel at the IUSTI laboratory (Institut Universitaire des Systèmes Thermiques Industriels, Marseille). Measurements of the time constant were taken in the free-stream of a 170 mm x 105 mm test section following a Mach 2 nozzle. The very low turbulence level in the free-stream together with controlled gas drying conditions are suitable for

the operation of hot-wire probes. The flow stagnation pressure was varied from 0.2 to 0.8 bar.

3 Results

3.1 Response time measurements

Figure 4(a) presents a typical response of the NSTAP sensor to the square wave test, and the methodology to compute the response time τ. Due to inherent flow unsteadiness from one period to another, a phase-average response was computed over more than 1000 periods to obtain the exponential growth corresponding to the increase of the sensor resistance. The phase-averaged response is exemplified in figure 4(b).

It was clear from all the experiments that the wire's voltage follows a first order linear system response:

$$E = C\left(1 - e^{-\frac{t}{\tau}}\right), \tag{1}$$

where the time constant τ represents the thermal inertia of the probe. To determine this thermal response, an exponential fit of the phase-averaged signals was implemented using equation 1, as exemplified in figure 4(b). The difference between the fit obtained either by the growth or the decrease of the sensor's resistance gives a good estimation of the error on τ. In both subsonic and supersonic conditions, the errors were found to be 3-5%.

Time constant measurements were performed for various overheat ratios between 0.06 and 0.8. Figure 5 depicts the evolution of the time constant for all sensors investigated. Noticeably, the response time of the nanoscale sensors is at least five times lower than the conventional cylindrical 5 μm-tungsten wire in both subsonic and supersonic flow configurations. Interestingly, the addition of gold layers monotonically decreases the NSTAP's response time down to $\tau = 20$ μs. This lowest value of τ was obtained for the gold-plated nanoscale probe with a gold layer of 360 nm, corresponding to a time constant reduction by a factor of 30 when compared to a classical 5 μm cylindrical probe.

In table 1, we summarize the values of τ averaged over a_w according to both the sensor and the flow configurations. We note that τ generally reduces for higher flow speeds, a fact that can be predicted from the unsteady heat equation over the probe (Bruun, 1995). This reduction, however, is negligible for the gold-plated NSTAP sensors. A detailed knowledge of the sensing element's resistance would be crucial to understand why the response time remains unchanged for subsonic and supersonic flow conditions when the gold layers are added.

Another point of interest is the effect of the flow condition associated with the overheat ratio on the response time.

Table 1 Averaged τ (μs) over a_w in subsonic and supersonic flows.

Sensor	Subsonic	Supersonic
5 μm cylindrical wire	678.7	526.3
NSTAP platinum	98.3	54.6
NSTAP platinum + 200 nm of gold	35.9	34.2
NSTAP platinum + 360 nm of gold	19.6	19.5

Although limited measurements were performed for supersonic flow conditions, figure 6 depicts the response time for both the conventional cylindrical and a gold-plated NSTAP for varying flow speed (i.e. total pressure P_0) and overheat ratio a_w. The 5 μm-probe presents a linear growth with a_w for both flow speeds. It is interesting to note that for increasing a_w, there is a decrease of the response time when the flow speed rises. Both the linear growth of τ with a_w and the nonlinear decrease of τ with flow speed can be predicted using a simple heat transfer model of a cylindrical hot-wire probe (Bruun, 1995). On the other hand, the gold-plated NSTAP probe presents no a_w dependence within the measurement uncertainties, but a decrease of τ with flow speed. While this behavior would be beneficial for experimental purposes and robustness to a_w variations, the physical reasons behind the difference between the cylindrical and the NSTAP probes remains to be elucidated.

4 Heat transfer analysis

In CCA operation without electronic compensation, the time constant is governed only by the thermal inertia of the sensor. The effect of the gold plating on the probe temperature profile is explored here using a heat transfer model and corresponding numerical simulations. In particular, we attempt to characterize how the temperature gradient changes in the vicinity of the sensing element.

4.1 Theoretical model

We consider a one-dimensional model along the sensor's length axis x following Bruun (1995). The equilibrium between the electrical heat generated by the Joule effect $\dot{Q}_e$ and the heat exchange by conduction $\dot{Q}_c$ and convection $\dot{Q}_h$ will be expressed for an incremental sensor element. The heat balance reads

$$d\dot{Q}_e = d\dot{Q}_h + d\dot{Q}_c + d\dot{Q}_s, \tag{2}$$

where $\dot{Q}_s$ is the heat stored by the sensor.

The generated heat by the traversing electric current I is given by:

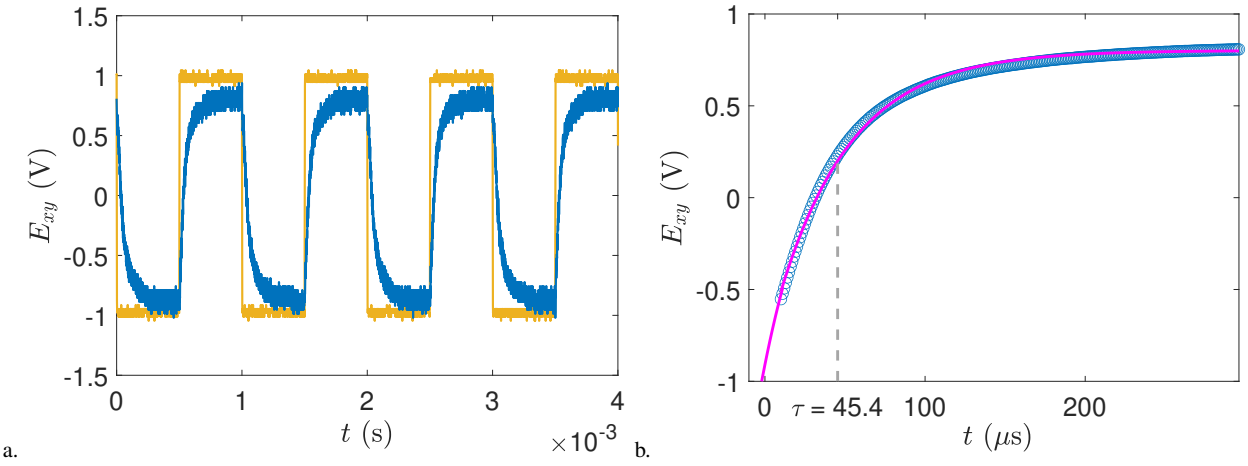

Fig. 4 a) Response of the NSTAP sensor (blue) to the square wave signal (yellow) due to step electrical current changes of 3.3 mA around the mean current of $I_o = 25.1$ mA. b) Phase-averaged wire voltage response and first-order exponential fit to compute the time constant τ using equation 1. In this example, the wire was placed in supersonic flow conditions: $M = 2$ and $P_0 = 0.8$ bar, the time constant was found to be $\tau = 45.4\,\mu$s for the conventional platinum NSTAP sensor.

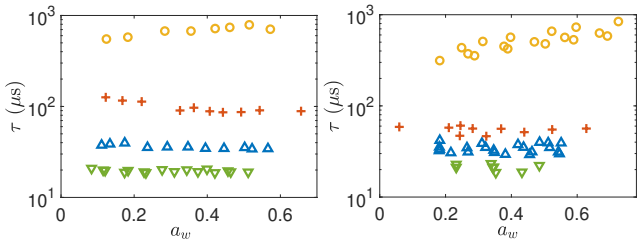

Fig. 5 Time constant in subsonic (left) and supersonic (right) flow conditions as a function of the overheat ratio a_w for the conventional 5 μm cylindrical probe (○), the conventional platinum NSTAP (+), the NSTAP with a 200 nm gold layer (△) and the NSTAP with a 360 nm gold layer (▽).

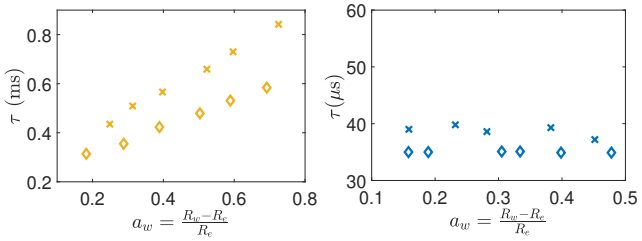

Fig. 6 Time constant evolution in supersonic flow as a function of the overheat ratio a_w for the classical 5 μm probe (left) and for the gold-plated NSTAP with a 200 nm gold layer (right) at different total pressure levels: open diamonds stand for $P_0 = 0.8$ bar and crosses stand for $P_0 = 0.4$ bar.

$$d\dot{Q}_e = dR_w I^2 = \frac{\chi_w(x,T(x))I^2}{A(x)}dx. \tag{3}$$

Here, $\chi_w(x,T)$ and $A(x)$ are the local electrical resistivity and cross section of the sensor, respectively, while $T(x)$ is the local wire temperature. The local resistivity χ_w is modelled by introducing the thermal coefficient of resistance α_0 and the resistivity χ_0 at $T_O = T_{293K}$:

$$\chi_w(x) = \chi_0\{1 + \alpha_0\,[T(x) - T_0]\}. \tag{4}$$

The heat convection from the wire to the flow is governed by the heat transfer coefficient, h, acting on the external surface S_w:

$$d\dot{Q}_h = h(x)S_w\,[T(x) - T_e]\,dx. \tag{5}$$

We consider $S_w = 2[w(x) + t]$ which takes into account both the upper and lower surfaces of the rectangular structure of the sensor.

Thermal conduction along the sensor is considered in the axial direction:

$$d\dot{Q}_c = -k_w A(x)\frac{\partial^2 T(x)}{\partial x^2}dx \tag{6}$$

and the heat storage is written as

$$d\dot{Q}_s = \rho_w C_p A(x)\frac{\partial T(x)}{\partial t}dx. \tag{7}$$

In the equations above, the density and heat capacity of the sensor's material are respectively ρ_w and C_p; the thermal conductivity is k_w. The equilibrium temperature of the unheated wire is T_e. Finally, the local width, the local cross-section and the sensor's thickness are $w(x)$, $A(x)$ and t, respectively

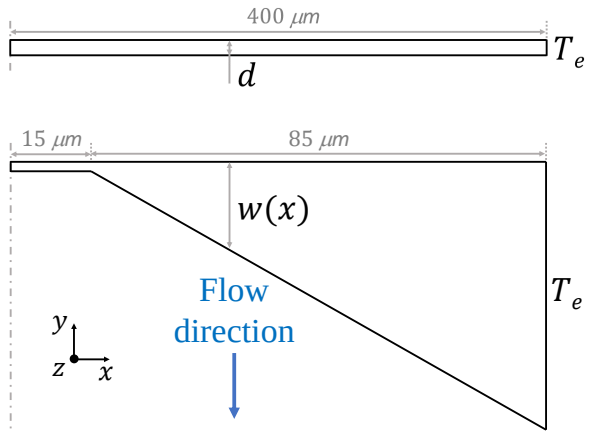

Fig. 7 Geometry of the cylindrical tungsten wire (d =5 μm, top) and the nanoscale probe (bottom) considered in the numerical simulations.

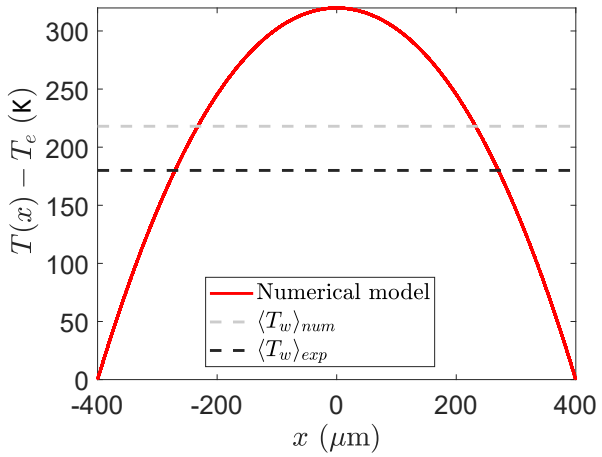

Fig. 8 Temperature profile along the 5 μm-tungsten wire computed from the numerical model (red curve) and its corresponding mean value $\langle T_w$ (dashed). The black dashed line represents the temperature estimated from the experimental data. For both cases, $a_w = 0.5$ and $R_w I^2 = 24$ mW.

4.2 Numerical simulation

The stationary solution of equations (2-7) provides the temperature profile across the sensing element and its vicinity. The problem consists in solving the heat transfer equations accounting for the geometry and materials of both a conventional cylindrical wire and the NSTAP sensors, which are sketched in figure 7. A Neumann condition is applied at the center of the wire, and the equilibrium temperature T_e is imposed at both extremities of the sensor. The equations were solved using the Finite Element Method (FEM), where the probe geometry was discretized in 1300 nodes. The sensor is surrounded by a low-speed air flow with free-stream velocity $u = 5$ m/s.

The convective heat transfer coefficient is modeled using a local Nusselt number:

$$h(x) = Nu \frac{k_f}{\ell(x)}, \tag{8}$$

where k_f is the fluid thermal conductivity and $\ell(x)$ the characteristic length scale in the flow direction. For a cylindrical wire, we set $\ell(x) = d$. For the ribbon shape of the NSTAP, we follow Kokmanian et al (2021) who considered both the width $w(x)$ and the thickness t. As the width w can be much larger than t and parallel to the fluid flow, we expect the most appropriate length scale $\ell(x) = w(x)$, which varies from 2 μm at the tip until approximately 50 μm at the vicinity of the sensing element (see figure 3 for the sensor's geometry). The Nusselt number employed here follows the King's law $Nu = A\sqrt{Re} + B$, with coefficients $A = 0.43$ and $B = 0.32$ empirically obtained for cylindrical hot-wires (McAdams, 1954). Here, the Reynolds number $Re = ul(x)/\nu$ is computed with the length scale $\ell(x)$ and the mean flow speed u of air with kinematic viscosity ν.

Table 2 Thermal and physical properties of materials at 293 K.

Mat.	C_p $[J.kg^{-1}.K^{-1}]$	ρ_w $[kg.m^{-3}]$	k_w $[W.m^{-1}.K^{-1}]$
Pt	130	21450	71.6
Au	128	19300	320
W	203	15630	174

The numerical model was first validated with the cylindrical 5 μm-tungsten wire. The temperature distribution along the wire axis $T(x)$ is shown in figure 8 for an arbitrary overheat ratio and electric power. The temperature profile agrees well with previous theoretical predictions examined in Bruun (1995). The mean temperature of the wire obtained numerically was $\langle T_w \rangle_{num} = 516K$. while the estimated temperature from the experiments was $\langle T_w \rangle_{exp} = 478K$. This difference might come from the experimental estimation that uses the measured wire resistance to compute the wire temperature:

$$\langle T_w \rangle_{exp} = \frac{R_w - R_e}{R_0 \alpha_0} + T_e \tag{9}$$

The model uses the resistivity of the wire to calculate the wire temperature that is integrated over the sensor's length.

To understand the effect of gold-plating on the heat transfer across the wire, simulations were performed for the NSTAP sensors matching the experimental conditions $I = 10$ mA for the platinum probe and $I = 12$ mA for the 360 nm gold plated sensor. These values correspond to the experiments conducted in the potential core of a jet with maximum flow speed $u = 5$ m.s^{-1}, coresponding to $R_w I^2 \simeq 3.8$ mW and $a_w \simeq 0.2$. For simplicity, only one half of the sensing element is solved as sketched in figure 7.

Figure 9 depicts the temperature profile $T(x)$ along the center-axis of the NSTAP probes. To better contrast the ef-

Table 3 Electric properties of the sensor's materials at 293 K.

Mat.	$\chi_0\ 10^{-6}[\Omega.m]$	$\alpha_0\ 10^{-3}[K^{-1}]$
Pt	0.1111	3.92
Au	0.0222	3.71
W	0.1124	3.68

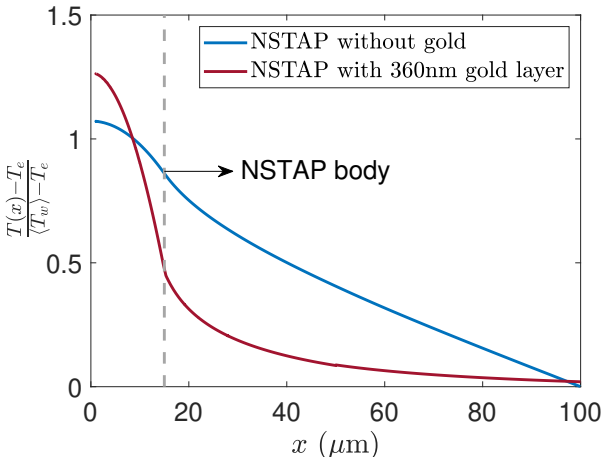

Fig. 9 Comparison of the numerical profile $T(x)-T_e$ normalized by the mean temperature of the sensing element $\langle T_w\rangle - T_e$ along the half length of the sensor with and without gold plating. The dashed line represent the limit between the ribbon-shaped sensing element and the supporting triangular structure.

fects of gold on the temperature profile, we normalize $T(x)-T_e$ by the average temperature of the sensing element (*i.e.* for $0 \leq x \leq 15$ μm for the half-sensor) subtracted by T_e. Without the presence of the gold layer, the curve presents a substantial sensor heating along the triangular structure ($15 \leq x \leq 100$ μm), which is highly attenuated by the presence of the 360 nm-metal layer. Hence, gold-plating mostly focuses the temperature gradient along the sensing element which directly reduces the response time of the sensor.

It is interesting to inquire to what extent this temperature profile is associated with end-conduction effects of the probe. For a cylindrical hot-wire, these effects can be quantified using the Γ parameter proposed by Hultmark et al (2011), which is defined based on the length-to-diameter ratio, the resistance ratio $a = R_w/R_e$, the Nusselt number Nu, the wire and the fluid thermal conductivity k_w and k_f, respectively. For the nanoscale ribbon geometry investigated here, the parameter assumes the following form (Byers, 2018):

$$\Gamma = \frac{l}{w}\sqrt{2a\left(\frac{k_f}{k_w}\right)\left(\frac{w+t}{t}\right)Nu} \tag{10}$$

where l, w and t stand for the length, the width and the thickness of the ribbon sensing element. Preliminary estimations of the Nusselt number reported by Kokmanian et al (2021) indicate $Nu \sim O(50)$, which would lead to a Γ parameter insufficiently small to avoid end-conduction effects. An extensive characterisation of the end-conduction effects for the present nanoscale geometry is hence necessary in future work, taking into consideration the exact values of the sensing element resistance, in spite of the entire probe impedance.

To localize the heat transfer on the sensing element, it is necessary to reduce the electrical heat production of the ribbon structure. As the heat production is proportional to $R_w I^2$, one would consider to reduce the local resistivity χ by adding a parallel conductor, here the gold-layer with thickness similar to the platinum structure. The gold-layer reduces the global resistivity by a factor $2\chi_{Au}/(\chi_{Pt}+\chi_{Au}) \simeq 0.33$. In addition, the thermal conductivity of the sensor is increased by a factor of almost 3 reducing the temperature variation between both extremities of the triangular supports at a constant heat production. The properties of all materials are presented in tables 2 and 3.

5 Numerical compensation of a turbulent flow signal

The addition of gold to the supporting structure focuses the temperature gradient into the sensing element, lowers the temperature of the stubs, hence reducing the response time of the probe. The decrease of the response time by an order of magnitude is associated with an equivalent increase of the sensor's frequency response. While in conventional operation of hot-wire probes in both CTA and CCA systems the signals are compensated with a parallel electronic circuit, one could inquire to what extent numerical compensation using the analytical first-order transfer function would provide reliable power spectral density results for the use of nanoscale probes in turbulent flows.

Given that the phase-averaged response signals show unambiguously the first-order nature of the sensor's response, the probe transfer function can be modeled as a low-pass filter. This is governed by the well-known transfer function:

$$H(j\omega) = \frac{1}{1+j\frac{\omega}{\omega_o}}. \tag{11}$$

ω is the angular frequency and ω_0 is the cut-off angular frequency defined as $\omega_0 = 1/\tau$. The resulting cut-off frequency is given by $f_0 = \omega_0/2\pi$. The transfer function gain G is the magnitude $\|H(j\omega)\|$. Using the conventional frequency variable $f = \omega/2\pi$, the frequency-dependent gain is computed as:

$$G(f) = \frac{1}{\sqrt{1+(f/f_0)^2}} \tag{12}$$

For a given power spectral density of a turbulent flow signal acquired without compensation, the compensated power

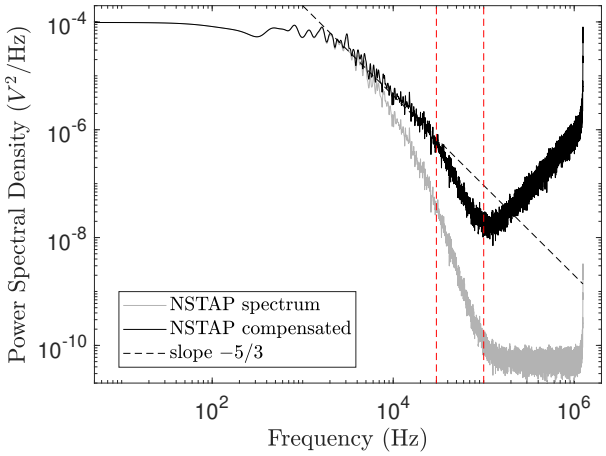

Fig. 10 Spectrum of the NSTAP with a gold layer of 200 nm. Red dashed lines represent the dissipation range and the cut-off frequency after compensation.

spectral density S_i is computed by the ratio between the measured power spectral density S_o and the squared gain $G(f)^2$.

To experimentally test the numerical compensation of a turbulent flow signal, the gold-plated nanoscale probe was placed in a high-subsonic jet issuing from a nozzle with an exit internal diameter $D_i = 4$ mm. The estimated jet flow speed based on static and stagnation pressure is $v = 105$ m/s. During the measurements, the probe was placed within the jet shear layer approximately four diameters downstream of the nozzle's outlet.

The power spectral density of hot-wire signals in this location should exhibit the universal $k^{-5/3}$ decay for more than one decade (Proença et al, 2019). Figure 10 presents the power spectral density (PSD) of both the original and the numerically compensated signals. It is important to note that the original signal was acquired using the CCA anemometer system described in section 2.1 without any compensation. Hence, in the PSD of the original signal, the rapid decay starting at approximately 4 kHz is due to the intrinsic thermal response of the nanoscale probe. This cut-off frequency agrees well with the response time $\tau = 30-40\,\mu$s presented in figure 5 for the 200 nm gold-plated probe. The compensated PSD shows a compelling $k^{-5/3}$ decay until 30 kHz where turbulent flow dissipation increases the decay rate until 100 kHz, which is the cut-off frequency of the compensated signal limited by the signal's noise originated from a digital converter of $N = 16$ bits.

6 Summary and conclusions

A constant current anemometer was built to characterize systematically the response time of nanoscale probes under multiple aerodynamic and overheat configurations. The experimental results show that the NSTAP probes present a response time at least one order of magnitude smaller than conventional cylindrical hot-wire probes. The associated frequency response shows similar features whether the probe is placed in subsonic or supersonic flow conditions, thus confirming the possibility of using the nanoscale probes in a variety of Mach number flows. It was shown that the time constant of the NSTAP sensors is insensitive to the overheat ratio, which is in contrast to the behavior of conventional hot-wire probes.

To explore the effects of the supporting structure on the sensor's frequency response, a gold layer was added at the vicinity of the sensing element over the original platinum structure. It demonstrates the possibility to control the response time by gold-plating, which focuses heat transfer along the nanoscale sensing element. The addition of gold-plating at the vicinity of the sensing element deserves further detailed investigations to find an optimal configuration considering both the response time and the end-conduction effects.

Finally, numerical compensation of acquired CCA signals without any electric compensation was successfully implemented in a high-speed turbulent flow. Due to the higher frequency response of the probe when compared to conventional hot-wires, the power spectral density of a turbulent flow signal can be computed over a large range of frequencies, which are limited only by the intrinsic noise of the acquisition system. In the tested experiments, a gold-plated nanoscale probe covers a spectral range until 100 kHz, paving the way for its application in a variety of flow conditions without the need of any sophisticated anemometer system with electric compensation.

Acknowledgements The authors gratefully thank Dr. Katherine Kokmanian for her advices during the preparation of the NSTAP probes.

Ethical Approval

Not applicable.

Availability of data and materials

Not applicable.

Competing interests

The authors declare no conflict of interest.

Authors' contributions

All authors wrote and reviewed the manuscript.

Funding

This work was supported by AFOSR/EOARD under the grant award FA8655-20-1-7040 monitored by Dr. Douglas R. Smith.

References

Bailey SC, Kunkel GJ, Hultmark M, Vallikivi M, Hill JP, Meyer KA, Tsay C, Arnold CB, Smits AJ (2010) Turbulence measurements using a nanoscale thermal anemometry probe. Journal of Fluid Mechanics 663:160–179

Bruun H (1995) Hot-wire anemometry: principles and signal analysis. Oxford Science Publications

Byers CP (2018) Theoretical and experimental investigations of similarity solutions in turbulent flows. PhD thesis, Princeton University

Comte-Bellot G (1976) Hot-wire anemometry. Annual Review of Fluid Mechanics 8(1):209–231

Féry A (1928) Etude de la variation de la résistivité des couches minces de platine en fonction de leur épaisseur et de l'influence des corps oxygénés sur de semblables resistances. Journal de Physique et le Radium 9(1):38–48

Hultmark M, Ashok A, Smits AJ (2011) A new criterion for end-conduction effects in hot-wire anemometry. Measurement Science and Technology 22(5):055,401

Hutchins N, Monty J, Hultmark M, Smits A (2015) A direct measure of the frequency response of hot-wire anemometers: temporal resolution issues in wall-bounded turbulence. Experiments in Fluids 56(1):1–18

King L (1914) On the convection of heat from small cylinders in a stream of fluid: Determination of the convection constants of small platinum wires with applications to hot-wire anemometry. Philosophical transactions of the royal society of London A 214(509-522):373–432

Kokmanian K, Scharnowski S, Bross M, Duvvuri S, Fu M, Kähler C, Hultmark M (2019) Development of a nanoscale hot-wire probe for supersonic flow applications. Experiments in Fluids 60(10):1–10

Kokmanian K, Barros D, Hultmark M, Dupont P (2021) Heat transfer measurements of a nanoscale hot-wire in supersonic flow. Experiments in Fluids 62(8):1–13

Kovasznay L (1950) The hot-wire anemometer in supersonic flow. Journal of the Aeronautical Sciences 17(9):565–572

Le-The H, Küchler C, van den Berg A, Bodenschatz E, Lohse D, Krug D (2021) Fabrication of freestanding pt nanowires for use as thermal anemometry probes in turbulence measurements. Microsystems & Nanoengineering 7(1):1–11

McAdams WH (1954) Heat Transmission, vol Chap. X. McGraw-Hill Book

Proença A, Lawrence J, Self R (2019) Measurements of the single-point and joint turbulence statistics of high subsonic jets using hot-wire anemometry. Experiments in Fluids 60(4):1–17

Schreyer AM, Lasserre JJ, Dupont P (2015) Development of a dual-PIV system for high-speed flow applications. Experiments in Fluids 56:187

Vallikivi M, Smits A (2014) Fabrication and characterization of a novel nanoscale thermal anemometry probe. Journal of Microelectromechanical Systems 23(4):899–907